Defect Identification Method of CMC Bonding Structure based on Dynamic Time Warping and Simulation Analysis

jiyang zhang
Changchun University of Science and Technology
jiaojiao ren (zimengrenjiao@163.com)
Changchun University of Science and Technology
dandan zhang
Changchun University of Science and Technology
jian gu
Changchun University of Science and Technology
lijuan li
Key Laboratory of Optoelectric Measurement and Optical Information Transmission Technology of the Ministry of Education
Tongyu Zhou
Changchun University of Science and Technology

Research Article

Keywords: Ceramic Matrix Composites (CMC), Dynamic Time Warping (DTW), Terahertz Nondestructive Testing, Transmission Matrix Method (TMM)

Posted Date: February 4th, 2021

DOI: https://doi.org/10.21203/rs.3.rs-154294/v1

Defect Identification Method of CMC Bonding Structure based on Dynamic Time Warping and Simulation Analysis

Jiyang Zhang[1,2], Jiaoyiao Ren[1,2,*], Lijuan Li[1,2], Jian Gu[1,2], Dandan Zhang[1,2], Tongyu Zhou[1,2]

[1]Changchun University of Science and Technolgoy, Changchun 130000, China.

[2]Key Laboratory of Optoelectric Measurement and Optical Information Transmission Technology of the Ministry of Education, Changchun 130000, China.

*Corresponding author.

E-mail address: 595868912@qq.com

Abstract

In this work, a new defect identification method has been proposed in an attempt to detect the bonding quality of ceramic matrix composites. The method is based entirely on dynamic time warping (DTW) and simulation analysis. Aiming at two different characteristic defects of the glue layer (I) and glue layer (II) of CMC, the transfer matrix method is employed to model and simulate the defects in the bonding structure. On the basis of this, a dynamic time warping algorithm is used to regularize the simulation waveform and the actual waveform in time sequence, and the correlation coefficient is employed for the estimation of waveform similarity after regularization. In comparison with the traditional similarity evaluation standard of the DTW algorithm, the improved DTW algorithm has better waveform classification ability for the glue layer (I) and glue layer (II). The classification accuracy of debonding defects of the glue layer (I) is more than 95%, and that of the glue layer (II) exceeds 90%. Additionally, compared with the conventional terahertz imaging method, correlation imaging is appropriate for different characteristics of defect signals and has an improved defect-recognition effect.

Keywords: Ceramic Matrix Composites (CMC), Dynamic Time Warping (DTW), Terahertz Nondestructive Testing, Transmission Matrix Method (TMM)

INTRODUCTION

Ceramic matrix composite (CMC) is a composite material composed of various fiber-reinforced ceramic substrates[1]. The key attributes of CMCs are their high stiffness, high-temperature resistance, lightweight and corrosion resistance, all of which hold immense importance in the aerospace field. Usually, a five-layer glue structure is formed using CMC, glue layer (I), insulating felt, glue layer (II), and metal substrate[2]. Therefore, the hidden debonding defects are understandably harmful to the bonding strength, and the detection accuracy and accuracy of these defects are the important standards to determine the system protection effectiveness in CMC materials. Nondestructive testing (NDT) technology is required to detect defects. The traditional nondestructive testing technologies include ultrasonic[3], eddy current[4], X-ray[5], etc., each having its own set of advantages and disadvantages. For example, the ultrasonic testing method may require a liquid coupling, and the detection resolution is relatively poor whereas eddy current technology is only able to detect surface and near-surface defects in conductive materials. X-ray method, on the other hand, is unsafe for the human body due to the involvement of the use of harmful radiation[6].

Terahertz wave is a kind of electromagnetic wave with a frequency ranging between 0.1 to 10 terahertz and as such lies between traditional microwave and infrared light waves[7]. THz time-domain spectroscopy (TDS) is one of the most popular THz methods. Owing to its strong penetrability and low photon energy radiation, it has great potential in the internal imaging of non-conductive and non-polar materials. These materials also include multilayer composites, which are opaque under visible and infrared light[8]. Besides, the inner layer thickness, the hidden defects, and inhomogeneity within these materials can be determined by the analysis

using THz radiation. It is worth noting that terahertz radiation provides a non-destructive, non-ionizing, and non-contact method for material evaluation[9].

There has been much research in recent years on nondestructive testing of CMC bonding structures using THz TDS. For the quality detection of glue layer of CMC bonding structure, the maximum value of the time-domain signal, flight time, variance, and other parameters are used for nondestructive testing signal analysis[10,11], whereas Fourier transforms, wavelet transform, EMD, and other methods are used to enhance weak signal[2,12], for improving the efficiency of defect identification. Simultaneously, in recent years, there have been some researches on the nondestructive detection of debonding defects of CMC materials using neural network intelligent recognition algorithm[1]. However, in the current research, the evaluation of glue defects of CMC samples is based on the analysis of a large number of standard samples. The terahertz signal characterization of different samples and defects is obtained via the analysis of a large number of samples. For individual samples, the information that can produce the best imaging effect must be determined separately, and different samples usually vary[13]. This immensely improves the difficulty of defect identification. A few works are based on the use of Finite Different Time Domain(FDTD)[14], Transfer Matrix Method (TMM), and other simulation methods[15] for analysis and research, but they only stayed in the theoretical analysis level, and are not sufficiently effective for the analysis for glue defects, and do not combine with the actual detection results.

Therefore, in an attempt to find a solution to the above problems, this paper proposes a defect identification method based on dynamic time warping and simulation analysis, the TMM is used to simulate the sampling waveform of the sample. The simulation was employed

to obtain the characteristic interval of the defect in the terahertz time domain. The DTW algorithm is used to time sequence the simulated waveform in the normal area. The actual waveform is then collected, and then the waveform similarity is calculated after regularization, which is utilized as the index of terahertz imaging.

PRINCIPLE

Terahertz Transmission Matrix Simulation

Because the test sample is usually a structure comprising multi-layers, considering the complexity of the structure, TMM is used to simulate. Each layer of TMM is modeled by the following two matrices:

The first matrix represents the behavior of terahertz signals at each interface between two media with different optical material constants, including the corresponding Fresnel coefficients[16].

$$D_{i,i+1} = \frac{1}{t_{i,i+1}} \begin{bmatrix} 1 & r_{i,i+1} \\ r_{i,i+1} & 1 \end{bmatrix} \tag{1}$$

where, $r_{i,i+1}$ and $t_{i,i+1}$ are Fresnel reflection and transmission coefficients respectively. The second matrix describes the propagation of the terahertz wave in the layer and represents the phase change of the incident terahertz signal.

$$P_i = \begin{bmatrix} e^{\frac{j\omega\tilde{n}_i d_i}{c}} & 0 \\ 0 & e^{\frac{-j\omega\tilde{n}_i d_i}{c}} \end{bmatrix} \tag{2}$$

where ω is the angular frequency, c is the speed of light, and $\tilde{n}_i$ is the complex refractive index of the layer ($\tilde{n}_i = n_i + j\kappa_i$). The whole theoretical transfer function $R(\omega)$ is obtained by

multiplying two matrices as follows:

$$M(\omega)=\prod_{i=0}^{k}P_i(\omega)\bullet D_{i,i+1}=\begin{bmatrix}M_{11}(\omega) & M_{12}(\omega)\\ M_{21}(\omega) & M_{22}(\omega)\end{bmatrix} \tag{3}$$

$$R(\omega)=\frac{M_{21}(\omega)}{M_{11}(\omega)} \tag{4}$$

Finally, the simulated terahertz time-domain signal can be obtained using the following formula[17]:

$$E(t)=F^{-1}(R(\omega)\bullet F(E_0(t))) \tag{5}$$

where, $F\left(E_0(t)\right)$ is the Fourier transform of incident THz pulse and F^{-1} is the inverse Fourier transform.

Calculation of Waveform Correlation Coefficient based on Dynamic Time Warping Algorithm

During the sample preparation process, the inhomogeneity of materials and the mutual penetration of glue layers leads to terahertz echo position shifting forward and backward in different regions. Traditional similarity calculation methods such as correlation coefficient, Manhattan distance, and Euclidean distance cannot be employed for calculation. Therefore, a similarity calculation method based on dynamic time warping is proposed in this paper. DTW is an algorithm to estimate the similarity between two sequences. The purpose of this measurement is to find the shortest path by twisting and bending a time series[18].

In the classic DTW algorithm, a local distance measure is defined to obtain the similarity between training samples and multiple test samples by finding the optimal path[19]. Assuming that there is a standard template r with length I and a training template t with length J, the optimal path is found through the Euclidean distance of each point of the standard template r and the training template t, resulting in finding the nonlinear matching between the

two templates[20], as shown in Fig. 1. The distance function $d(i,j)$ is Euclidean distance, which is usually employed for the measurement of similarity. The regularized path D can be described as follows:

$$D = \left\{ d(i(q), j(q)) \middle| \begin{array}{c} q = 1,...,Q \\ \max(I,J) \le Q \le I + J - 1 \end{array} \right\} \tag{6}$$

Boundary conditions, continuity, monotonicity, and slope constraints have to be satisfied when selecting the path[21]. The similarity $Dist(t,r)$ between the training template and test template can be obtained using the path D. The minimum total distance of the regular path is the best alignment between the test sample and the training sample.

$$Dist(t,r) = \min \left(\frac{\sum_{q=1}^{Q} d(i(q), j(q))}{Q} \right) \tag{7}$$

Among them, the shortest distance regular path rw and tw can be found through the normalization coefficient by backtracking[22].

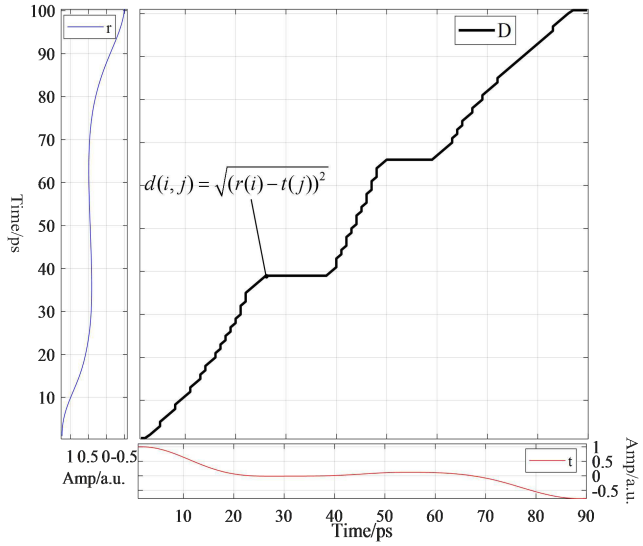

Figure 1. Warping grid using Euclidian distance.

However, the uncertainty in the actual manufacturing process of materials gives rise to a morphological difference between the actual and simulation waveform. The conventional

method of calculation of Euclidean distance will result in a large difference between the normal and the simulation waveform, which is hard to be distinguished from the defective waveform. Therefore, this paper focuses on calculating the Pearson correlation coefficient of the regular path rw and tw as the final measure of similarity between the standard template and the training template[23], The formula is as follows.

$$p = \frac{Cov(rw, tw)}{\sigma_{rw}\sigma_{tw}} \tag{8}$$

where $Cov(rw,tw)$ is the covariance of the regularized path whereas σ_{rw}, σ_{tw} are the standard deviations of rw and tw, respectively.

ANALYSIS AND DISCUSSION OF EXPERIMENTAL RESULTS

Sample Production and Signal Analysis

The sample employed in this paper is a ceramic matrix composite bonding sample represented in Fig. 2, and usually comprises CMC, glue layer (I), insulating material, glue layer (II), and metal substrate. The bonding process involves the glue layer (I)s being applied on the surface of CMC, the upper and lower surfaces of insulating materials, and the surface of the metal substrate. This is followed by the application of the glue layer (I)s from the middle to the edge. During the sample production process, a semicircular polytetrafluoroethylene membrane having a thickness of 0.15mm and a diameter of 20mm is preset in the glue layer (I), whereas a similar semicircular polytetrafluoroethylene membrane 0.25mm thick and 20mm in diameter is preset on the four sides of the glue layer (II). Following the solidification of the glue layer, it is extracted to simulate the debonding defect[24].

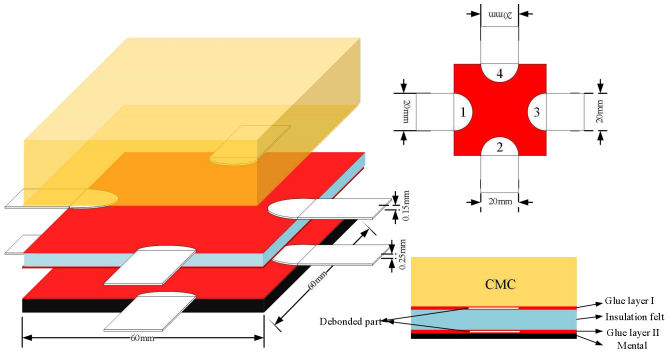

Figure 2. Sample design and dimensions.

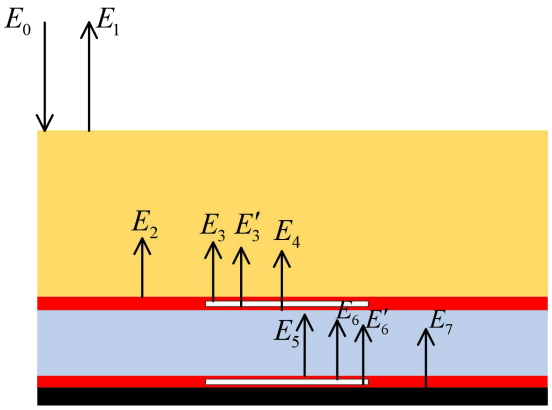

Figure 3. Schematic of terahertz signal in reflection mode.

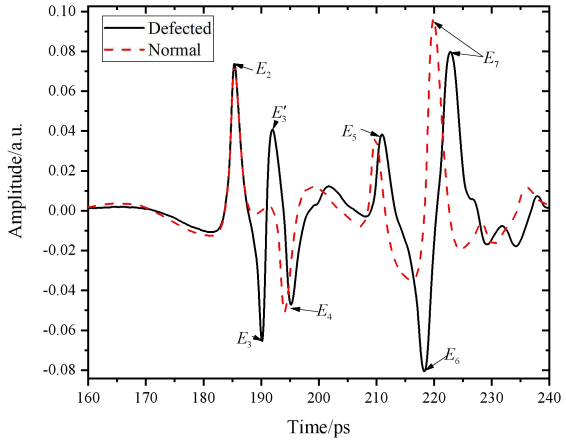

Figure 4. Simulated THz time-domain waveforms of defected and normal location.

Fig. 3 shows the reflection of the theoretical THz wave at each interface of the specimen.

The above TMM matrix is used to obtain the simulation waveforms of the defect and normal region as shown in Fig. 4. In the figure, the simulation waveform simulates the time-domain waveform reflected from the samples with and without defects, which carries the major portion of the information from the time-domain. Generally speaking, when an electromagnetic wave is reflected from the interface between incident material and reflective material with a higher refractive index than incident material, phase inversion will occur. When the incident wave encounters a reflective material with a lower refractive index than the incident material, the phase change of the reflected wave interface will not occur[25]. Due to the thickness of the sample, the time delay of the reflected wave E_1 from the upper surface usually exceeds the maximum time delay (320 ps) of our system upon focusing on the glue layer. Then, the reflected signal E_2 from CMC material to the glue layer (I) is the most obvious signal. E_3 represents the reflection signals from the upper surface of a defect in glue layer (I), E_4 from glue layer (I) to insulating material whereas E_5 and E_6 are from insulating material to the upper surface of defect II and glue layer (II), respectively. Reflected signals from the lower surface of defects are represented by E_3' and E_6'. However, for E_6', most of them will be mixed into the reflection peak (E_7) at the bottom of the metal substrate. Therefore, it can be easily inferred that the waveform of the debonding defect of the glue layer (I) lies between E_2 and E_4 whereas the debonding defects of the glue layer (II) lie between E_5 and E_7. Therefore, the characteristic intervals between the upper and lower defect can be selected for local matching in the light of the simulation waveform. The simulation waveform implies that the debonding defect of the glue layer (I) is characterized by the peak and valley after E_2 which is essentially the significant feature, while the debonding defect of the glue layer (II) is characterized by the

deepening of the back valley of E_5 and is the fuzzy feature.

Terahertz Signal Classification and Recognition

The terahertz time-domain spectrum system was employed to collect 100 terahertz time-domain waveforms of the normal and defective areas. The waveform intervals of glue layer (I) and glue layer (II), namely E_2 and E_4, E_6 and E_7 were selected respectively. By the analysis of the flight time of glue layer (I) and glue layer (II) in a normal area, it is evident that the thickness of glue layer (I) and (II) is different, and certain differences exist in the waveform shape, which may be a result of uneven coating and glue penetration.

The thickness of the glue layer (I) is often greater than that of the glue layer (II) due to the difference in the amount of glue. Therefore, the time of flight of glue layer (I) is about 9-11.5 ps for the layer (II) whereas the flight time is about 3-5.5ps. DTW algorithm is used for time warping, as shown in Fig. 5 and Fig. 6, and it is evident that dynamic time warping has a certain regularization effect on glue layer (I) and (II). A better matching effect can be achieved because the local waveform can align the position of the characteristic peaks, which, for subsequent data processing is more convenient. For the glue layer (I), 9.5ps-10ps has a good regularity effect; for glue layer (II), a good regularity effect exists in the range of 4ps-5ps. However, when the flight time deviates from the optimal regularization range, the traditional DTW method using Euclidean distance to evaluate waveform similarity can be no longer applied. Therefore, this paper makes use of the Pearson correlation coefficient as a means to evaluate the waveform similarity after regularization.

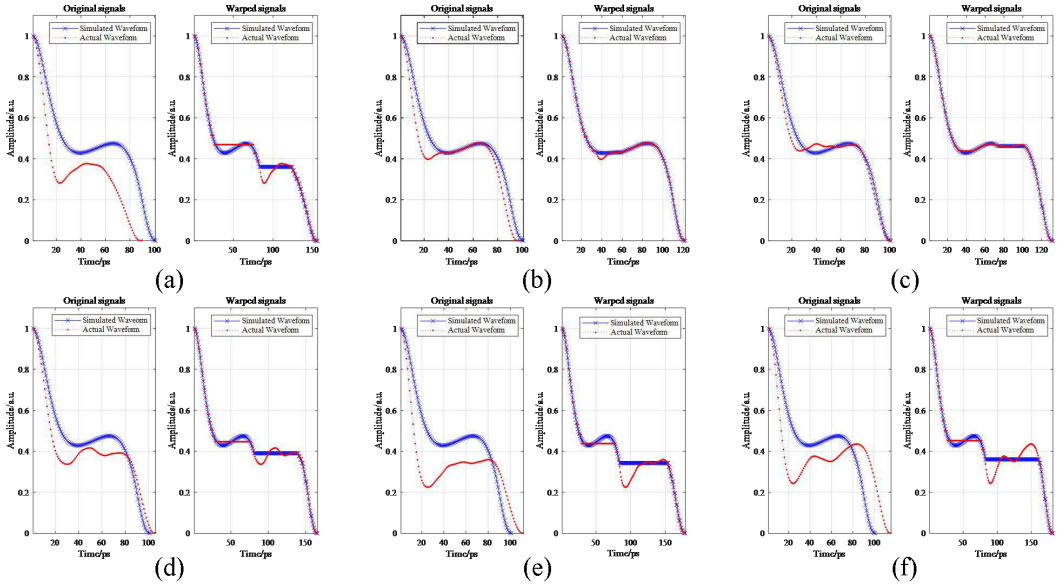

Figure 5. The comparison of the original signals and the warped signals of different thickness of glue layer (I): (a) 9ps, (b) 9.5ps, (c) 10ps, (d) 10.5ps, (e) 11ps, (f) 11.5ps.

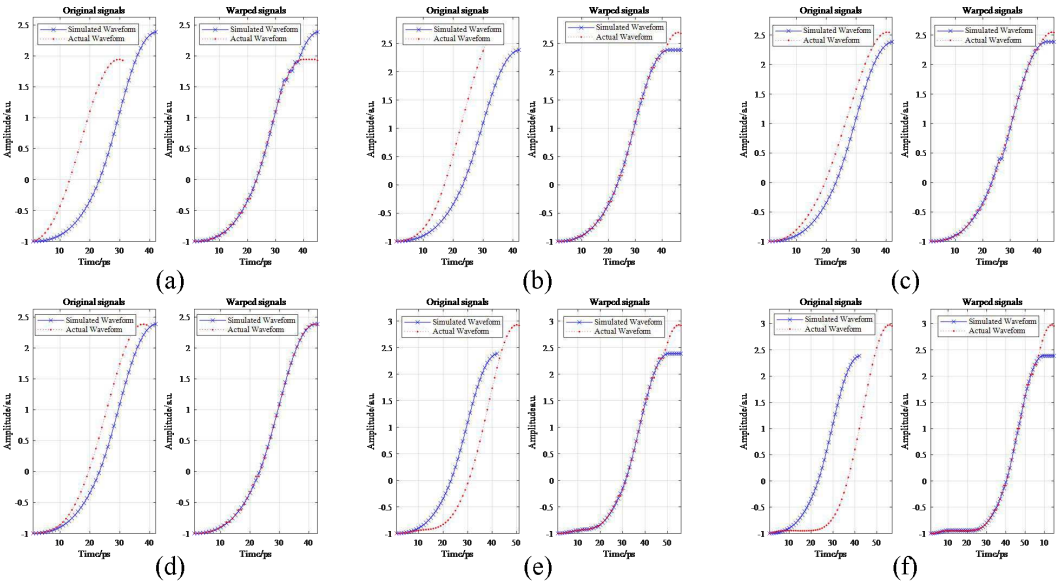

Figure 6. The comparison of the original signals and the warped signals of different thickness of glue layer (II): (a) 3ps, (b) 3.5ps, (c) 4ps, (d) 4.5ps, (e) 5ps, (f) 5.5ps.

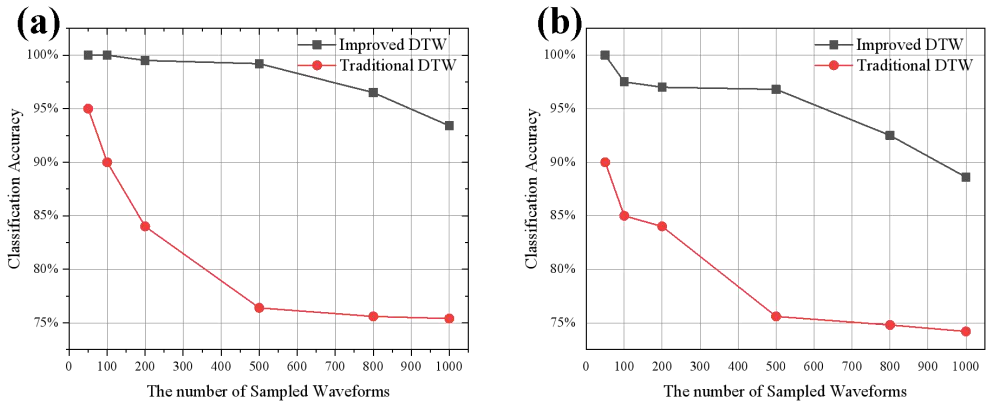

Figure 7. The classification accuracy curve for different debonding defect with DTW algorithm and the improved DTW algorithm: (a) Glue layer (I) debonding defect, (b) Glue layer (II) debonding defect.

In an attempt to verify the capability of the dynamic time warping algorithm in the light of the Pearson correlation coefficient for classifying and recognizing glue debonding defects, two dynamic time warping algorithms were used to respectively classify the different waveforms of different sampled quantities. The results are shown in Fig. 7 where (a) is the classification accuracy curve of glue layer (I) debonding defects (b) is the classification accuracy curve of the glue layer (II) debonding defects.

As evident in Fig. 7, with the increase of sampling quantity, the classification accuracy of both algorithms decreases. This is because the edge area of the material affects the classification accuracy. While both algorithms have a good classification recognition effect for debonding defects of glue layer (I), the traditional DTW algorithm uses Euclidean distance to calculate its similarity and the difference of waveform pattern caused by the thickness of different regions causes the accuracy of the Euclidean distance algorithm to decrease. Hence with the increase of sampling number, the accuracy of the traditional DTW algorithm

waveform classification decreases significantly and the stability also becomes lower. The improved DTW algorithm pays more attention to the change in waveform trend; the debonding defects of the glue layer (I) and (II) have a good recognition effect. There is, thus, a noteworthy improvement in the standard deviation of the identification as well as the stability of the waveform classification. The classification accuracy of the debonding defect of the glue layer (I) is more than 95%, and the classification accuracy of the debonding defect of the glue layer (II) exceeds 90%.

Correlation Imaging based on Dynamic Time Warping

The traditional imaging method and correlation imaging method are employed to image and analyze the defects of the glue layer (I) and (II) of the sample. The images are shown in Fig. 8, Figs. 8 (a) and (b) are the maximum imaging and correlation imaging map of debonding defect glue layer (I) whereas (c) and (d) are the minimum imaging and correlation image of debonding defects of the glue layer (II). The red and yellow areas in the figure represent the defect area, while the normal area is represented as blue.

It is evident that in case of obvious defect characteristics, such as debonding defect of the glue layer (I), there isn't an overall obvious difference between the traditional maximum value imaging and correlation imaging, however, the correlation imaging has a good recognition effect for the four side defects, while the maximum value imaging manifests a poor recognition effect for upper and lower defects, which may be the result of the unknown maximum value characteristics caused by the difference in materials used for the preparation of samples. Obviously, for the debonding defects of the glue layer (II), the defect characteristics are fuzzier, and the defect identification is more influenced by the material inhomogeneity and dispersion.

Therefore, the traditional minimum value imaging effect is not good, however, the correlation imaging method can make up for this defect, and also exhibits a good recognition effect for debonding defects of the glue layer (II).

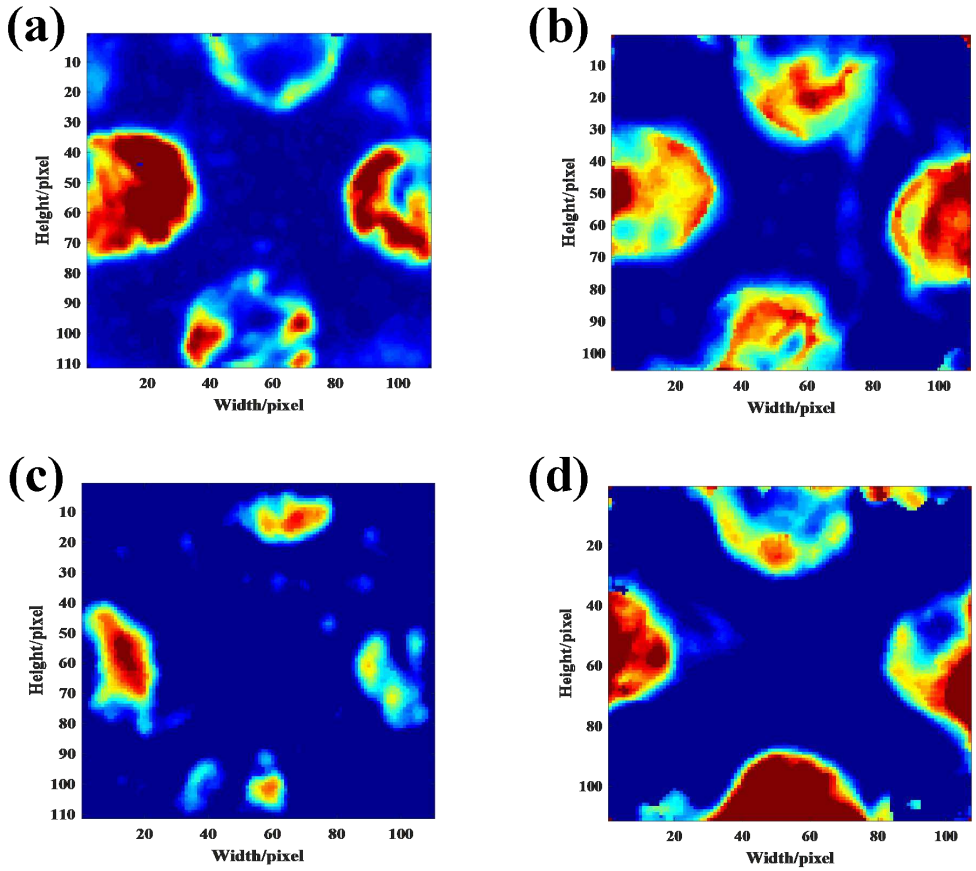

Figure 8. Different images of debonding defects: (a) Maximum imaging of glue layer (I), (b) Correlation imaging of glue layer (I), (c) Minimum imaging of glue layer (II), (d) Correlation imaging of glue layer (II).

CONCLUSIONS

In this study, a defect identification method based on dynamic time warping and simulation analysis is proposed, which primarily aims at two different types of defect detection in ceramic matrix composite glue materials. The defect characteristics and characteristic

intervals of the simulation waveform analyzer are obtained based on the TMM method. The method not only provides theoretical support for terahertz non-destructive testing but also reduces the dependence of traditional nondestructive testing on standard samples. Besides, to solve the problem of position shift of terahertz echo caused by material non-uniform penetration and scattering, a DTW algorithm based on Pearson correlation coefficient is proposed. Compared with the traditional DTW algorithm, the improved method is more suitable for terahertz signals and shows a better classification effect in the process of defected waveform recognition. It has higher defect-recognition rate. Finally, a new imaging recognition algorithm has been proposed in this paper which focuses on the identification of debonding defects existing in the glue layer (I) and glue layer (II) in the CMC bonding structure. Pearson correlation coefficient is used to carry out correlation imaging. Compared with traditional THz single feature imaging, the correlation imaging method has better imaging recognition ability for debonding defects of glue layer (I) and glue layer (II). However, for defect detection, the edge recognition ability still needs to be improved.

REFERENCES

1. Ren, J. *et al*. Study on intelligent recognition detection technology of debond defects for ceramic matrix composites based on terahertz time domain spectroscopy. *Appl. Opt.* **55**, 7204-7211 (2016).
2. Dai, B. *et al*. Improved terahertz nondestructive detection of debonds locating in layered structures based on wavelet transform. *Compos. Struct.* **168**, 562-568 (2017).
3. Chen, H. L., Zhang, B., Alvin, M. A. & Lin， Y. Ultrasonic detection of delamination and

material characterization of thermal barrier coatings. *J. Therm. Spray Technol.* **21**, 1184-1194 (2012).

4. Yong, L., Chen, Z., Mao, Y. & Yong, Q. Quantitative evaluation of thermal barrier coating based on eddy current technique. *NDT E Int.* **50**, 29-35 (2012).
5. Ullmann, T. *et al*. Quality assurance for the manufacturing of oxide fiber reinforced ceramic composites for aerospace applications. in *4th International Symposium on NDT in Aerospace*, Augsburg, Deutschland, 2012, pp. 1-11.
6. Kolbe, M., Beckhoff, B., Krumrey, M. & Ulm, G. Thickness determination for Cu and Ni nanolayers: Comparison of completely reference-free fundamental parameter-based X-ray fluorescence analysis and X-ray reflectometry. *Spectrochim. Acta B At. Spectrosc.* **60**, 505-510 (2005).
7. Singh, S. P., Akhter, Z. & Akhtar, M. J. Calibration independent estimation of optical constants using terahertz time‐domain spectroscopy. *Microw. Opt. Technol. Lett.* **57**, 1861-1864 (2015).
8. Wang, Q. *et al*. Nondestructive imaging of hidden defects in aircraft sandwich composites using terahertz time-domain spectroscopy. *Infrared Phys. Technol.* **97**, 326-340 (2019).
9. Chang, T., Guo, Q., Liu, L. & Cui, H. L. Nondestructive thickness inspection of capsule coating by terahertz time-domain spectroscopy. *IEEE Trans. Terahertz Sci. Technol.* **8**, 688-695 (2018).
10. Zhang, J. *et al*. Nondestructive evaluation of glass fiber honeycomb sandwich panels using reflective terahertz imaging. *J. Sandw. Struct. Mater.* **21**, 1211-1223 (2019).
11. Zhang, D. D. *et al.* Nondestructive testing of bonding defects in multilayered ceramic

matrix composites using THz time domain spectroscopy and imaging. *Compos. Struct.* **251**, 112624 (2020).

12. Qiao, X. *et al*. Mean estimation empirical mode decomposition method for terahertz time-domain spectroscopy de-noising. *Appl. Opt.* **56**, 7138-7145 (2017).
13. Dong, J., Wu, X., Locquet, A. & Citrin, D. S. Terahertz superresolution stratigraphic characterization of multilayered structures using sparse deconvolution. *IEEE Trans. Terahertz Sci. Technol.* **7**, 260-267 (2017).
14. Tu, W., Zhong, S., Shen, Y., Zhou, Q. & Yao, L. FDTD-based quantitative analysis of terahertz wave detection for multilayered structures. *J. Opt. Soc. Am. A Opt. Image Sci. Vis.* **31**, 2285-2293 (2014).
15. Krimi, S. *et al*. Highly accurate thickness measurement of multi-layered automotive paints using terahertz technology. *Appl. Phys. Lett.* **109**, 021105 (2016).
16. Palka, N. *et al*. Precise determination of thicknesses of multilayer polyethylene composite materials by terahertz time-domain spectroscopy. *J. Infrared Millim. Terahertz Waves* **36**, 578-596 (2015).
17. Duvillaret, L., Garet, F. & Coutaz, J. L. A reliable method for extraction of material parameters in terahertz time-domain spectroscopy. *IEEE J. Sel. Top. Quant. Electron.* **2**, 739-746 (1996).
18. Mueen, A. & Keogh, E. Extracting optimal performance from dynamic time warping. In: *Proceedings of the 22nd ACM SIGKDD International Conference on Knowledge Discovery and Data Mining*, 2016, pp. 2129-2130.
19. Cheng, H., Dai, Z., Liu, Z. & Zhao, Y. An image-to-class dynamic time warping approach

for both 3D static and trajectory hand gesture recognition. *Pattern Recognit.* **55**, 137-147 (2016).

20. Zhou, Z., Cao, Z. & Pi, Y. Dynamic gesture recognition with a terahertz radar based on range profile sequences and Doppler signatures. *Sensors* **18**, 10 (2018).
21. Ko, M. H., West, G., Venkatesh, S. & Kumar, M. Using dynamic time warping for online temporal fusion in multisensor systems. *Inform. Fusion* **9**, 370-388 (2008).
22. Salvador, S. & Chan, P. Toward accurate dynamic time warping in linear time and space. *Intell. Data Anal.* **11**, 561-580 (2007).
23. Hauke, J. & Kossowski, T. Comparison of values of Pearson's and Spearman's correlation coefficients on the same sets of data. *Quaestiones Geographicae* **30**, 87-93 (2011).
24. Xu, F., Duan Mu, Q. D., Li, L. J., Yang, D. & Xia, B. Nondestructive evaluation of rubber composites using terahertz time domain spectroscopy. *Fibres Text. East. Eur.* **26**, 67-72 (2018).
25. Wu, D., Haude, C., Burger, R. & Peters, O. Application of terahertz time domain spectroscopy for NDT of oxide-oxide ceramic matrix composites. *Infrared Phys. Technol.* **102**, 102995 (2019).

ACKNOWLEDGEMENTS

This work is also supported by Jilin Province Science and Technology Resources Open Sharing Service Platform and Scientific Research Condition Guarantee Project (201910040022TC), Jilin Province Science and Technology Development Plan Project (201506230147C), and Youth Innovation Fund Project of Changchun University of Science

and Technology (XJJLG-2018-03).

AUTHOR CONTRIBUTIONS

Jiyang zhang and Jiaojiao Ren wrote the main manuscript，Lijuan Li prepared figures 3-4. Dandan Zhang and Jian Gu prepared the experimental samples and collected the data. All authors reviewed the manuscript.

COMPETING INTERESTS

The authors declare no competing interests.

Figures

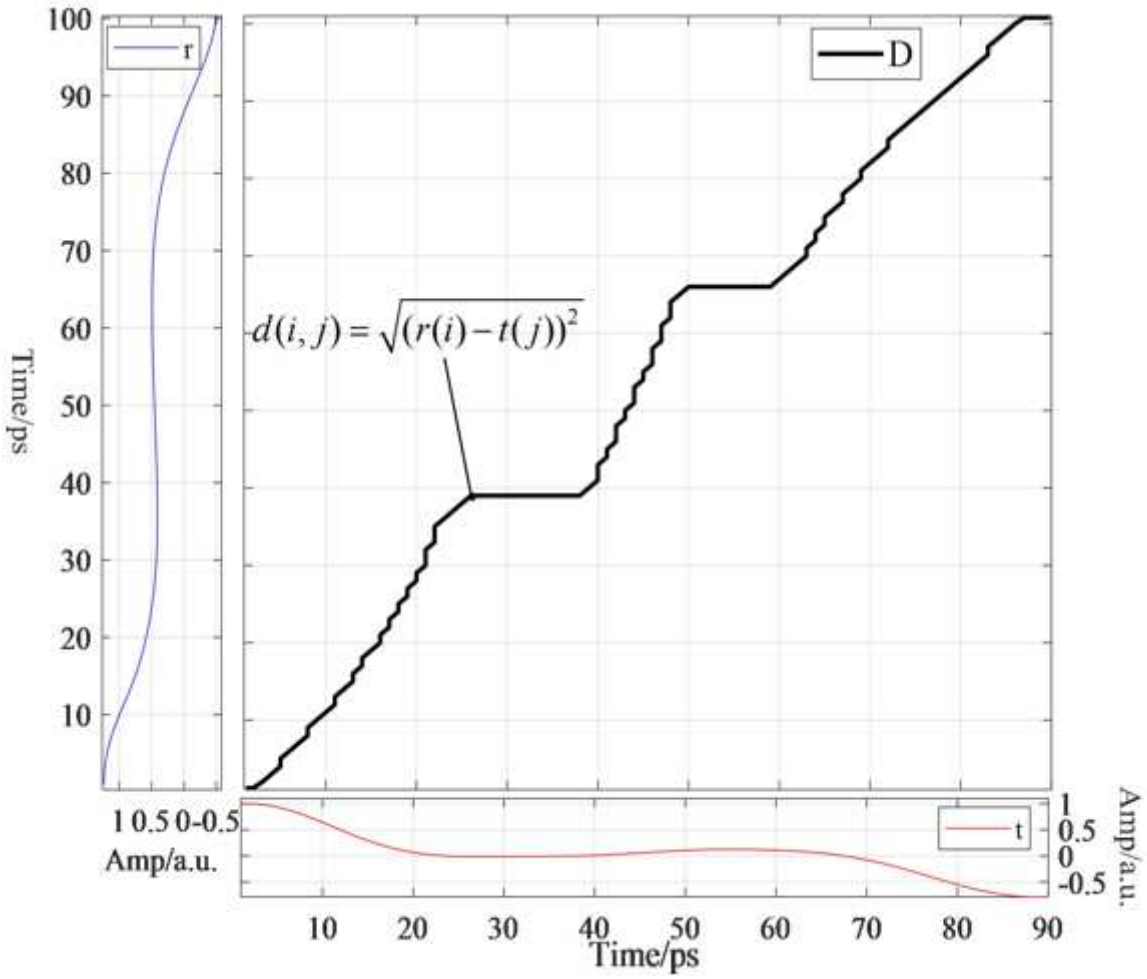

Figure 1

Warping grid using Euclidian distance.

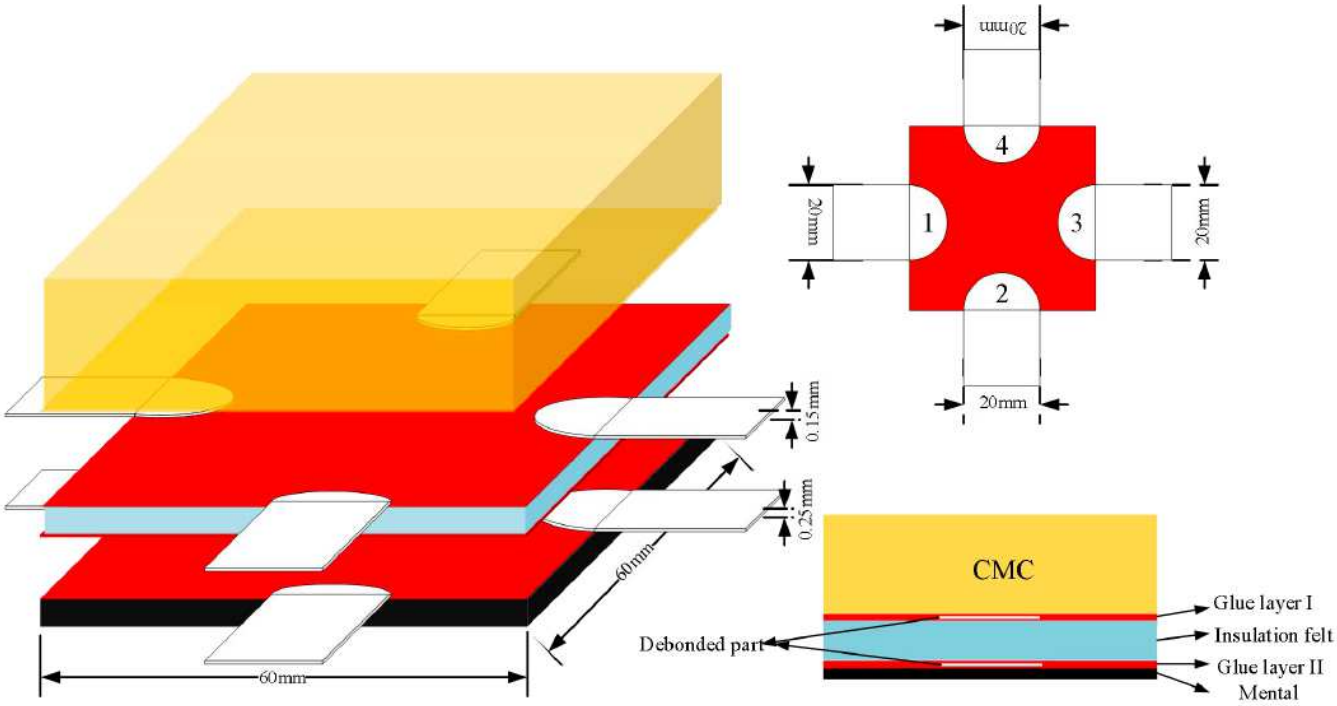

Figure 2

Warping grid using Euclidian distance.

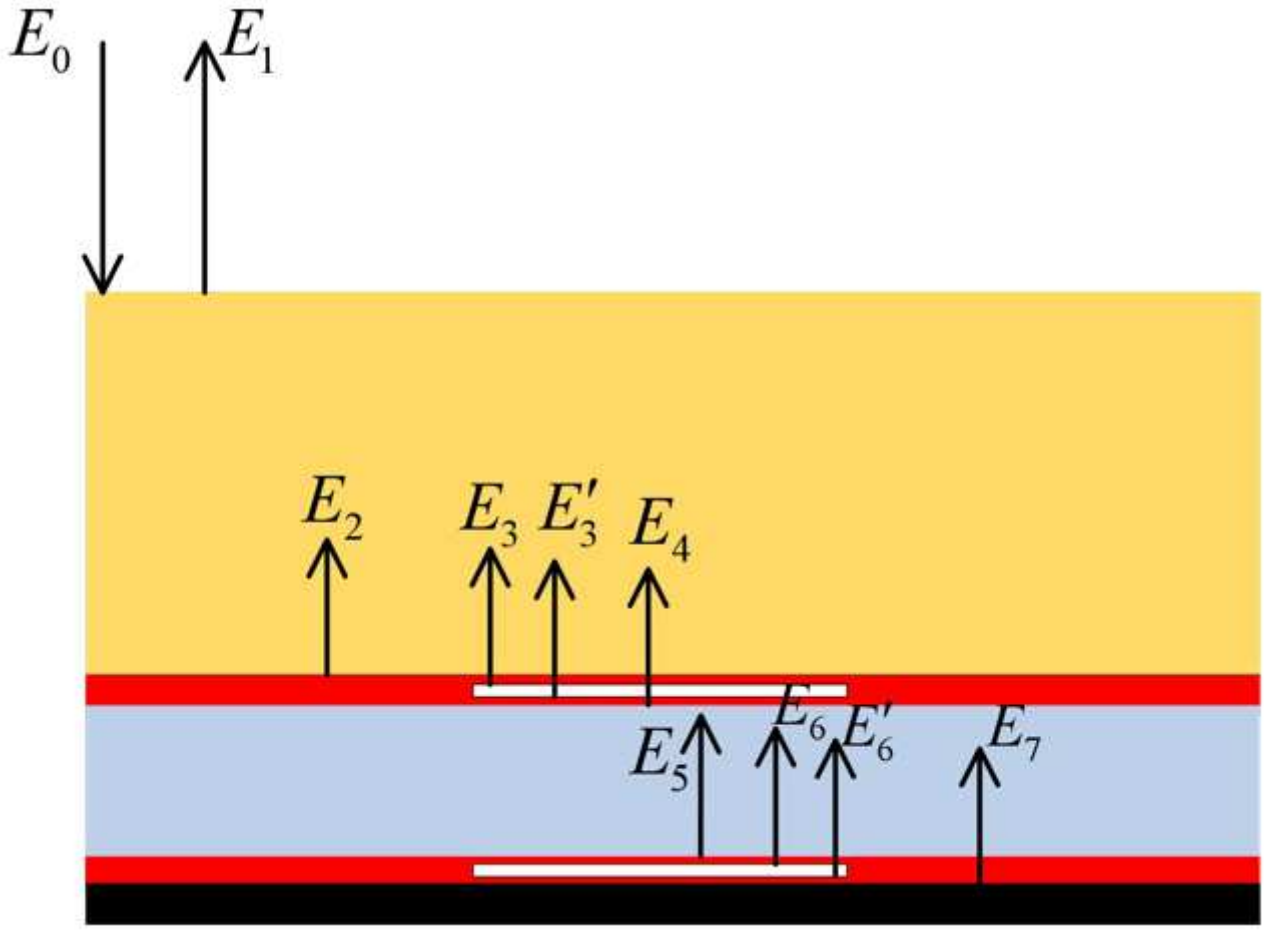

Figure 3

Schematic of terahertz signal in reflection mode.

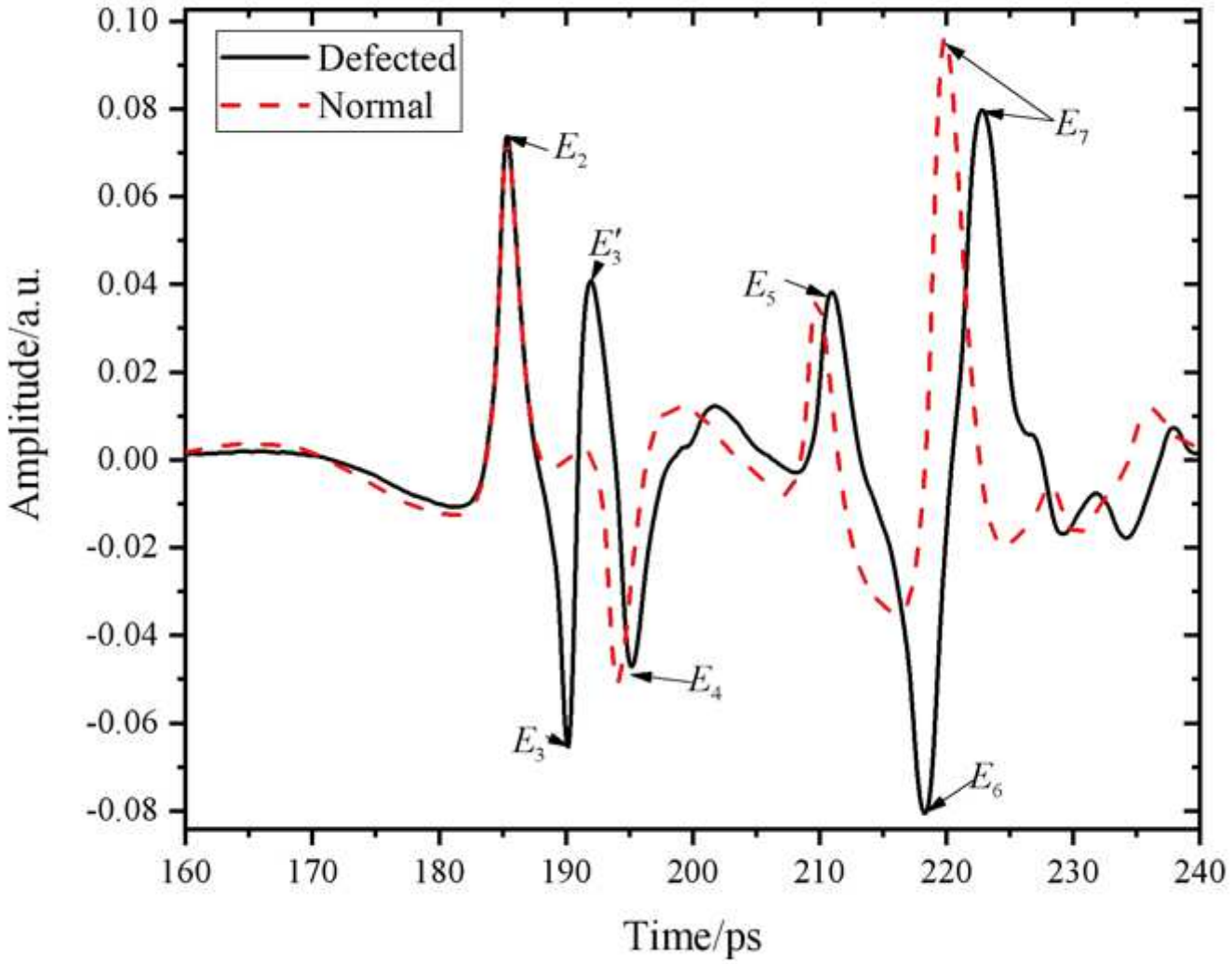

Figure 4

Simulated THz time-domain waveforms of defected and normal location.

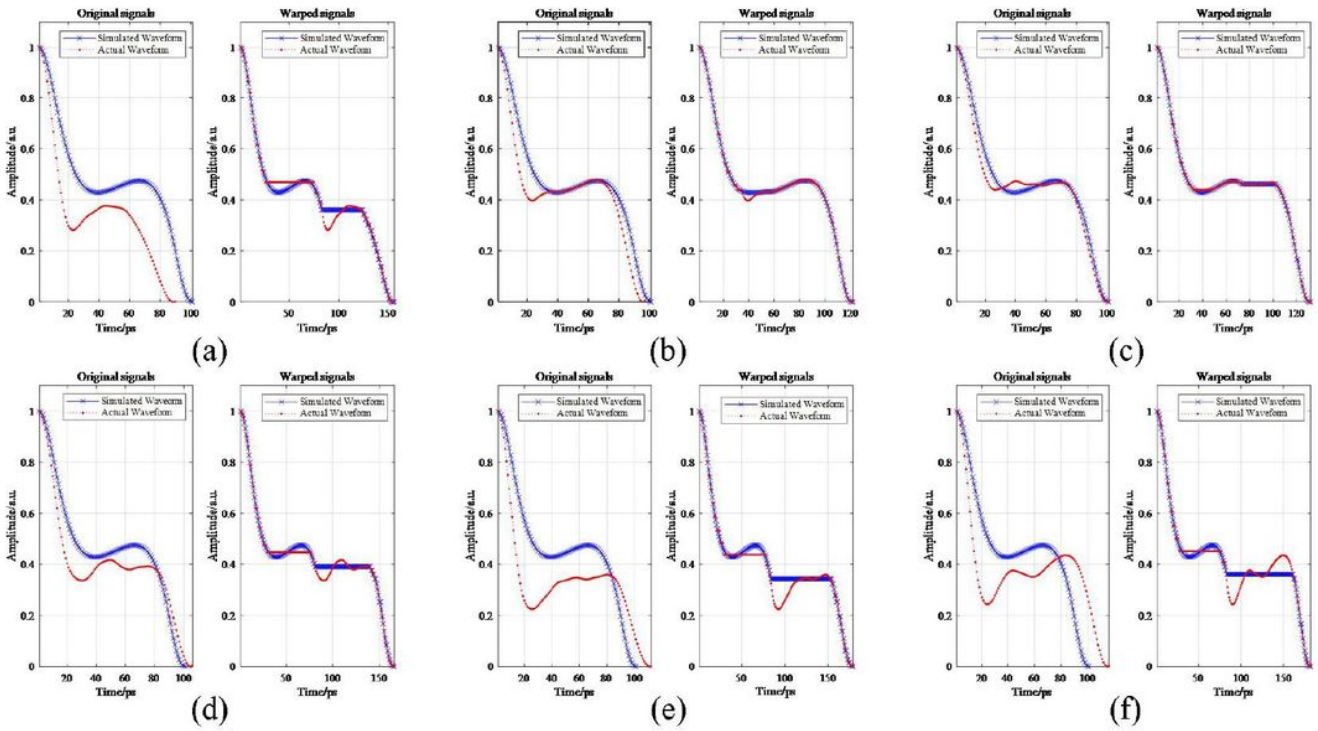

Figure 5

The comparison of the original signals and the warped signals of different thickness of glue layer (l): (a) 9ps, (b) 9.5ps, (c) 10ps, (d) 10.5ps, (e) 11ps, (f) 11.5ps.

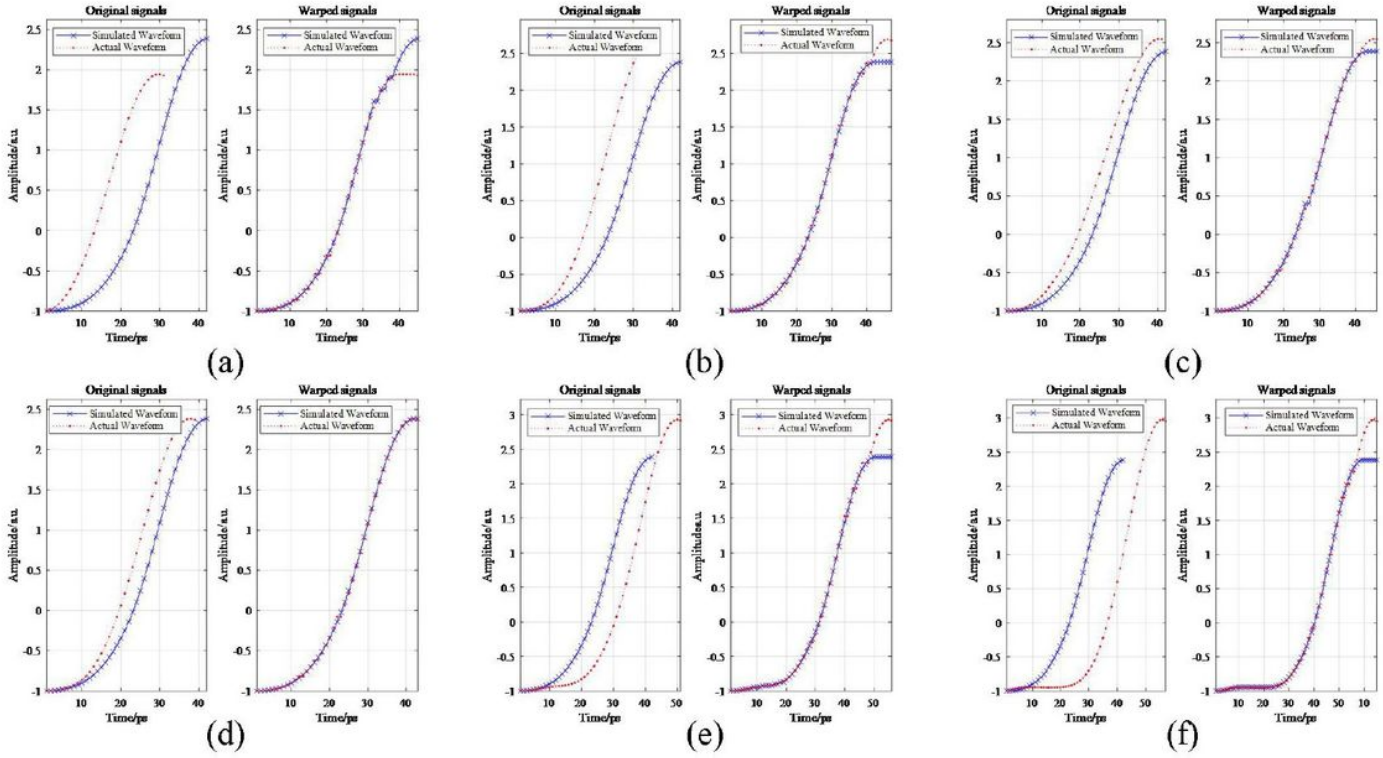

Figure 6

The comparison of the original signals and the warped signals of different thickness of glue layer (II): (a) 3ps, (b) 3.5ps, (c) 4ps, (d) 4.5ps, (e) 5ps, (f) 5.5ps.

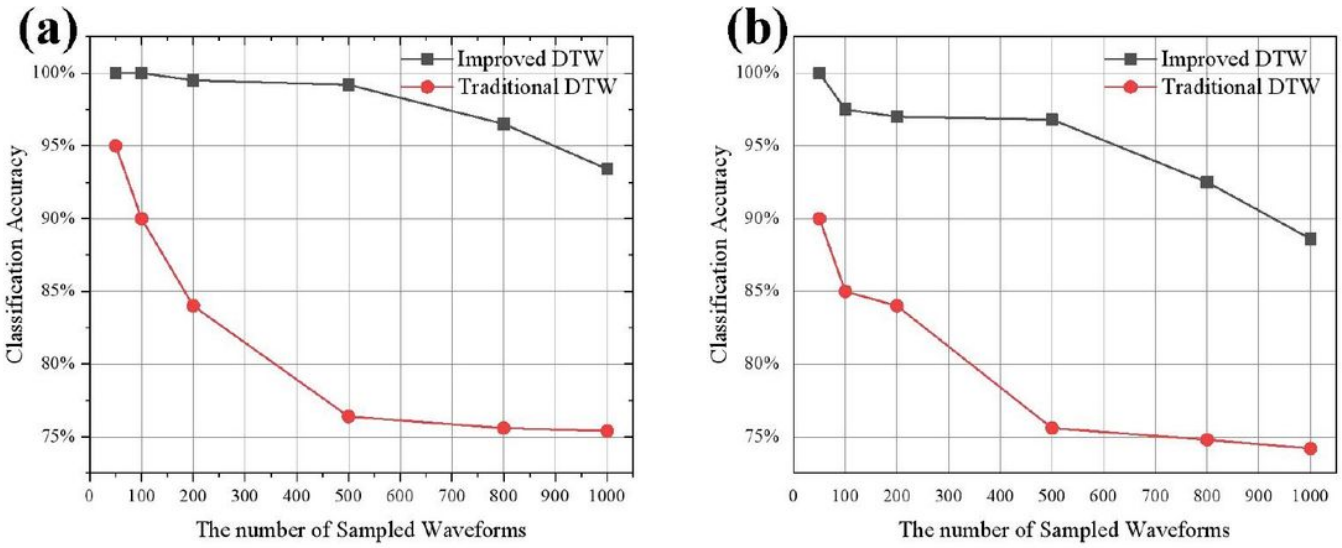

Figure 7

The classification accuracy curve for different debonding defect with DTW algorithm and the improved DTW algorithm: (a) Glue layer (I) debonding defect, (b) Glue layer (II) debonding defect.

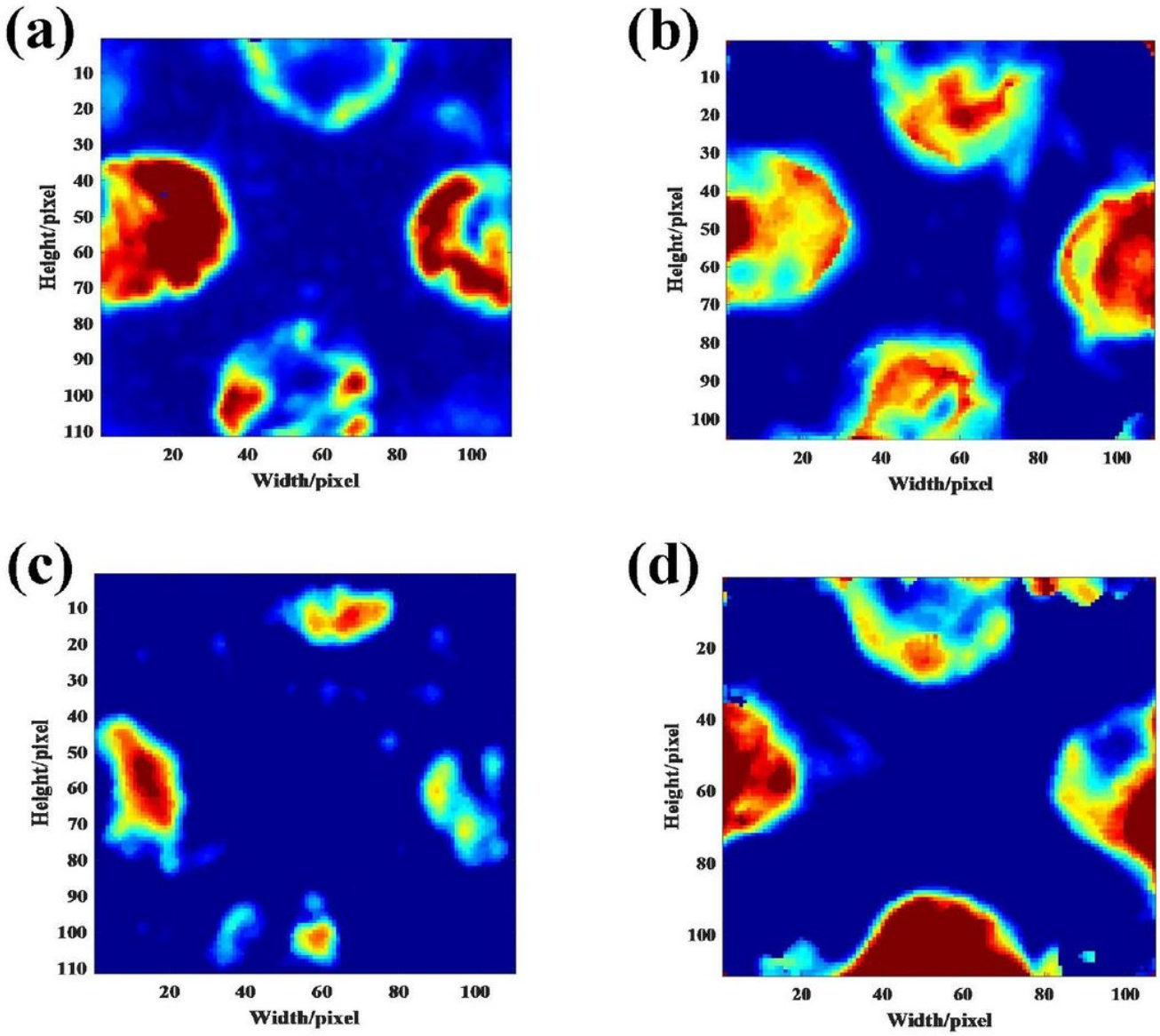

Figure 8

Different images of debonding defects: (a) Maximum imaging of glue layer (I), (b) Correlation imaging of glue layer (I), (c) Minimum imaging of glue layer (II), (d) Correlation imaging of glue layer (II).